[6] Mario Tosi, in *Solid State Physics*, edited by F. Seitz and D. Turnbull (Academic, New York, 1965), Vol. 16.

[7] R. D. Shannon and C. T. Prewitt, Acta Cryst. B25, 925 (1969). The scale denoted *IR* or *VI* coordination has been taken here. This corresponds most nearly to the Pauling ionic radii which were taken in Refs. 2 and 3.

[8] A. Kiel and W. B. Mims, Phys. Rev. B 5, 803 (1972).

[9] R. J. Elliott and K. W. Stevens, Proc. Roy. Soc. (London) A218, 553 (1953).

[10] The replacement of operators such as $V_{\text{odd}}|\psi_u\rangle\langle\psi_u|\delta V_{\text{odd}}$ with an equivalent even-field operator is discussed by A. Kiel, Phys. Rev. 148, 247 (1966). The argument has been reproduced schematically here in order to make it clear that in second order the odd fields can remix pure J states belonging to a ground manifold thus leaving a_{jk} and g_{jk} proportional as in Eq. (9), and giving $F_{ijk}=\eta T_{ijk}$ as in Eq. (10).

PHYSICAL REVIEW B VOLUME 5, NUMBER 9 1 MAY 1972

Magnetic Properties of Granular Nickel Films

J. I. Gittleman, Y. Goldstein,* and S. Bozowski
RCA Laboratories, Princeton, New Jersey 08540

(Received 10 September 1971)

Granular films, about 1 μ thick and ranging in composition from 20–90-vol% nickel were prepared by cosputtering nickel and quartz. Electron micrography and diffraction show the specimens to be composed of nickel particles (~ 50 Å in diameter) embedded in a matrix of SiO_2. The electrical resistivity increased from about 10^{-4} Ω cm at 90-vol% Ni to about 10^{-2} Ω cm at 50 vol%. Measurements were made of the magnetoresistance and the magnetic field dependence of the Kerr rotation as a function of temperature and composition of the Ni-SiO_2 system. These measurements provide evidence that the granular Ni-SiO_2 system can exist in three possible magnetic phases. At sufficiently high temperatures each nickel grain is paramagnetic. At lower temperatures the ensemble is superparamagnetic with each grain being ferromagnetic but with the magnetic moments of neighboring grains weakly correlated. At sufficiently low temperature the ensemble of grains becomes ferromagnetic, the moment of each grain being highly correlated with those of its neighbors. Our magnetoresistance measurements show that the electron tunneling probability is spin dependent.

I. INTRODUCTION

Granular metals have received wide attention recently.[1–4] It was found that these materials exhibited anomalously large resistivities which were attributed to the fact that the material is composed of individual metal grains embedded in an insulating matrix with the conduction dominated by electron tunneling between grains.[2,3,5,6] Such a system represents an ensemble of weakly coupled tiny metal particles which, in the case of superconductivity, exhibited striking properties.[1,5,7] In the case of a granular ferromagnet, the ferromagnetic properties are expected to be affected both by the metal grain size[8,9] and by the strength of the coupling between particles.

This paper presents a systematic study of the magnetic properties of the Ni-SiO_2 system. We measured the magnetoresistance and the magnetization as a function of temperature and composition of the Ni-SiO_2 system and preliminary results have been published.[10] Our data are in agreement with the accepted tunneling model but in addition show that the electron tunneling probability is spin dependent. An anomaly in the temperature dependence of the magnetoresistance for specimens with nickel concentrations in the neighborhood of 50 vol% was observed which we associate with a highly composition-dependent ordering temperature T_M. We interpret T_M as separating two phases. For $T > T_M$, the magnetic system behaves as an array of independent, uncorrelated magnetic moments (superparamagnetic). For $T < T_M$ the system as a whole behaves ferromagnetically with all of the moments highly correlated. The symbol T_M is used to avoid confusion with T_C, the Curie temperature of the individual grains.

II. EXPERIMENTAL METHODS

The Ni-SiO_2 samples were cosputtered from Ni and SiO_2 targets on fused-quartz substrates. The relative volume composition of Ni and SiO_2 were determined from thickness measurements as described by Hanak and Gittleman and Hanak.[7] The specimens were usually about 1 μ thick, 0.25–0.75 cm wide, 13 cm long, had an average concentration gradient (along the long dimension) of about 6 vol% per cm and ranged in concentration from 20–90 vol% Ni. The specimens used for resistivity measurements had contacts of narrow gold strips deposited at 0.25-cm intervals across the Ni-SiO_2 films. This is shown in Fig. 1 which is a photograph of an actual specimen. Electron micrography and diffraction show the specimens to be composed of fcc nickel particles imbedded in a matrix of SiO_2 similar to the case of other granular metals.[1,2,3,7] Diffraction lines characteristic of nickel oxide or other compounds of Ni were not observed. The estimated grain size from electron-microscopy measurements was 50–60 Å.

A. Resistivity and Magnetoresistance

The resistance of the samples ranged from a fraction of an Ω to 10^9 Ω and higher depending on Ni concentration and temperature. Whenever feasible a four-contact method was employed to measure the sample resistance. The high-resistivity samples were measured with a dc Wheatstone bridge, ascertaining first that rectification effects due to contacts were negligible. The bridge method was employed also for measuring the relative magnetoresistance $\Delta\rho/\rho_0$, where $\Delta\rho$ is the change of the resistivity due to a magnetic field and ρ_0 is the resistivity in the absence of a field. The specimens were mounted on a heavy copper block enclosed by a protective can which was part of the sample-holder arrangement and could be evacuated. To vary the temperature, the sample holder was immersed into a glass Dewar containing a coolant liquid. The coolant liquids used were helium, nitrogen, various grades of freon, and water. In addition the specimens could be heated by an electrical heater. The temperature of the specimen was determined by measuring the temperature of the coolant and the temperature difference between the coolant and the copper mounting block with a thermocouple. For transverse magnetoresistance measurements the Dewar was inserted between the poles of a conventional electromagnet. The field was applied parallel to the specimen surface but perpendicular to the direction of the current flow. For the longitudinal magnetoresistance measurements we used a superconducting magnet with its axis parallel to the current flow. The magnetic fields were measured by using calibrated Hall probes.

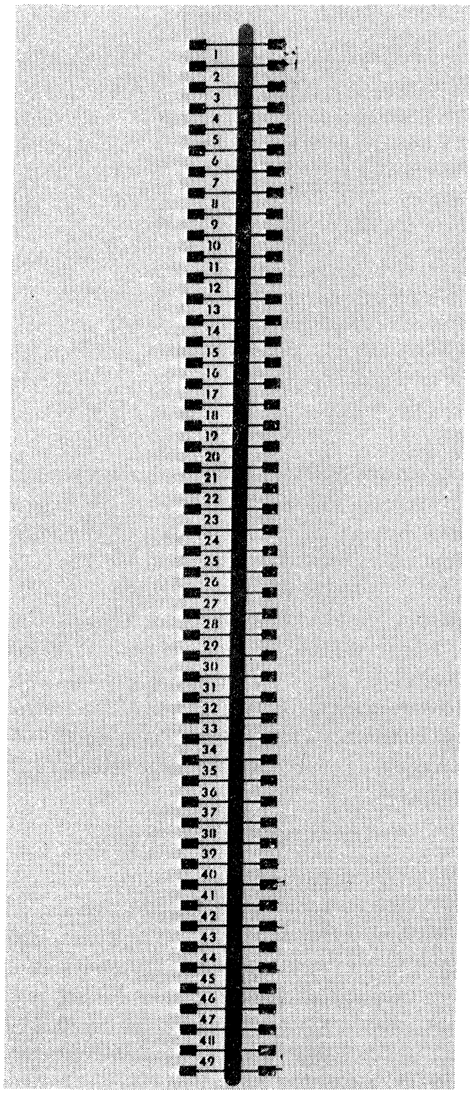

FIG. 1. Sputtered Ni-SiO_2 specimen. Sample No. 1, SiO_2 rich; sample No. 49, Ni rich.

B. Magneto-Optic Measurements

To measure the magneto-optical Kerr effect we used a polarization-modulation technique developed by Jasperson and Schnatterly.[11] This method is very sensitive and angles of rotation of the order of 1 min can be measured easily. The schematic of the experimental set-up is shown in Fig. 2. A light beam from a monochromator passes through a linear polarizer (LP), modulator (M) and impinges on the sample. The reflected beam is analyzed with a linear analyzer (LA) and is detected by a silicon detector. The angle between the incident and reflected beam was kept less than 1°. The specimens were mounted similarly as for the magnetoresistance measurements. However, in this case there was a small hole in the protective can to allow the light beam to pass through. No windows were mounted on the protective can to avoid any spurious rotations due to the Faraday effect of the window material. Because of this the specimens could not be cooled and only moderately heated (up to about 360 °K). The inner part of the sample holder could be moved vertically, by means of a calibrated precision screw, to align the different samples with the light beam. The magnet used was a conventional electromagnet with a small hole through one of the poles.

The modulator consists of an optically polished fused quartz block of about $5\times 2\times 1$ cm^3, bonded to a similar block of single-crystal quartz. The dimensions of both the quartz blocks were chosen such that their fundamental resonant frequency for longitudinal sound waves should be equal and around 50 kHz. An electric signal, at the resonant frequency, applied to the quartz crystal generates a standing (sound) wave along the long dimension in both quartz blocks. Due to this uniaxial strain wave in the fused quartz, the index of refraction for light polarized along the strain direction varies periodically. Denoting this direction by $\vec{\mathrm{j}}$ and the perpendicular to it by $\vec{\mathrm{i}}$, we can write the amplitude $\vec{\mathrm{E}}$ of the incident light polarized 45° with respect to the $\vec{\mathrm{i}}$ and $\vec{\mathrm{j}}$ axes, as

$$\vec{\mathrm{E}} = 2E_0(\vec{\mathrm{i}}+\vec{\mathrm{j}}) \ . \tag{1}$$

After passing through the modulator the $\vec{\mathrm{j}}$ component of the light phase shifted relative to the $\vec{\mathrm{i}}$ component by an angle δ and the transmitted amplitude $\vec{\mathrm{E}}_t$ can be written as

$$\begin{aligned}\vec{\mathrm{E}}_t &= 2E_0(\vec{\mathrm{i}}+e^{i\delta}\vec{\mathrm{j}})\\ &= E_0\left[(1-ie^{i\delta})(\vec{\mathrm{i}}+i\vec{\mathrm{j}})+(1+ie^{i\delta})(\vec{\mathrm{i}}-i\vec{\mathrm{j}})\right] \ ,\end{aligned} \tag{2}$$

where $i=(-1)^{1/2}$. The phase shift δ is given by

$$\delta = A\sin\omega t \ , \tag{3}$$

where ω is the (angular) sound frequency and the relative phase amplitude A is proportional to the thickness of the quartz block and to V/λ, where V is the applied ac voltage and λ is the wavelength of the light.

After reflection from a magnetized opaque film at perpendicular incidence, the reflected amplitude $\vec{\mathrm{E}}_r$ is given by

$$\vec{\mathrm{E}}_r = E_0\left[r_+(1-ie^{i\delta})(\vec{\mathrm{i}}+i\vec{\mathrm{j}})+r_-(1+ie^{i\delta})(\vec{\mathrm{i}}-i\vec{\mathrm{j}})\right] \ , \tag{4}$$

where r_+ and r_- are the reflection coefficients for right and left circularly polarized light, respectively:

$$r_+=(1-n_+)/(1+n_+) \ , \quad r_-=(1-n_-)/(1+n_-) \ . \tag{5}$$

Here n_+ and n_-, the (complex) indices of refraction for right and left circularly polarized light, respectively, are given by

$$n_+^2=\kappa_1+i\kappa_2 \ , \quad n_-^2=\kappa_1-i\kappa_2 \ . \tag{6}$$

Here κ_1 is the (complex) dielectric constant at the absence of magnetization and κ_2 is proportional to the magnetization.[12] Analyzing the reflected light with a linear analyzer whose axis is at 45° to the axis of the initial polarizer (i.e., along the $\vec{\mathrm{i}}$ or $\vec{\mathrm{j}}$ direction), we can write for the intensity I_r^{45}

$$I_r^{45}\propto |E_{r\vec{\mathrm{i}}}|^2=|E_{r\vec{\mathrm{j}}}|^2 \ , \tag{7}$$

which yields

$$I_r^{45}=2CE_0^2(|r_+^2|+|r_-^2|)(1-2\phi_\kappa\cos\delta-2\epsilon_\kappa\sin\delta) \ . \tag{8}$$

Here ϕ_κ and ϵ_κ are the Kerr rotation angle and ellipticity respectively,[12] given by

$$\phi_\kappa=\mathrm{Im}\left(\frac{n_--n_+}{n_+n_--1}\right) , \quad \epsilon_\kappa=\mathrm{Re}\left(\frac{n_--n_+}{n_+n_--1}\right) \ , \tag{9}$$

and C is a proportionality constant. Using Eq. (3) and expanding $\cos\delta$ and $\sin\delta$ in Bessel functions we obtain

$$\cos\delta=J_0(A)+2J_2(A)\cos2\omega t+2J_4(A)\cos4\omega t+\cdots \ , \tag{10}$$

$$\sin\delta=2J_1(A)\sin\omega t+2J_3(A)\sin3\omega t+\cdots \ . \tag{11}$$

Substituting Eqs. (10) and (11) into Eq. (8) we obtain

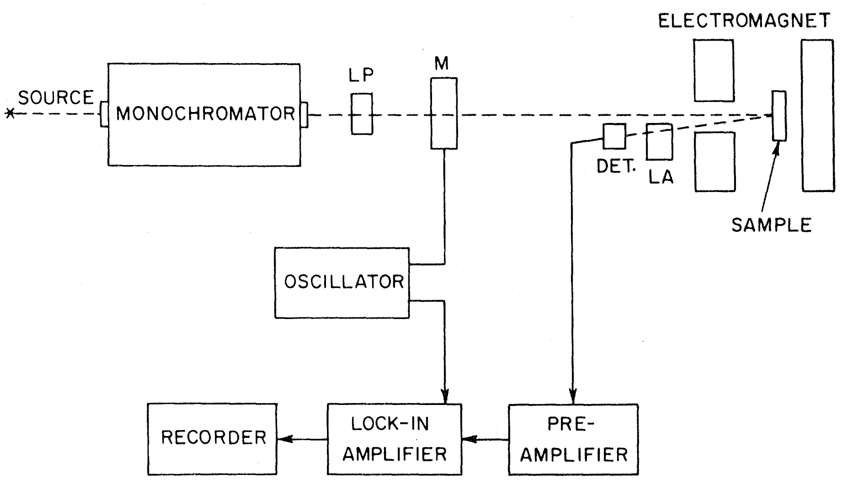

FIG. 2. Schematic diagram of arrangement for measuring the magneto-optical Kerr effect.

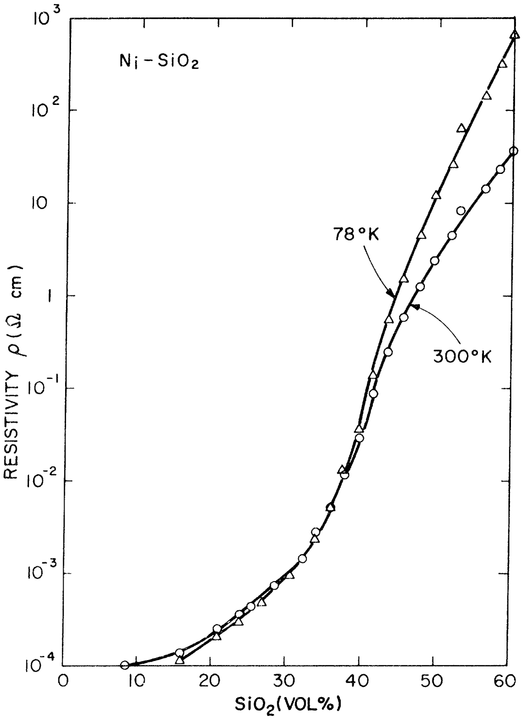

FIG. 3. Resistivity of Ni-SiO_2 vs composition.

$$I_r^{45}=2CE_0^2(|r_+^2|+|r_-^2|)$$

$$\times(1-2\phi_\kappa J_0(A)-4\phi_\kappa J_2(A)\cos 2\omega t$$

$$-4\epsilon_\kappa J_1(A)\sin\omega t+\cdots)\ . \qquad (12)$$

Thus by measuring the amplitude of I_r^{45} at the fundamental frequency ω and at the second harmonic 2ω one can measure ϵ_κ and ϕ_κ. To eliminate the constants appearing in Eq. (12) one can measure the analyzed light intensity I_r^0 with the analyzer parallel to the polarizer. In this case

$$I_r^0\propto\tfrac{1}{2}\,|E_{r\vec{i}}\,E_{r\vec{j}}\,|^2\ , \qquad (13)$$

which becomes

$$I_r^0=2CE_0^2(\,|r_+^2|+(r_-^2|\,)$$

$$\times(1+\cos\delta-2\epsilon_\kappa\sin\delta-|\epsilon_\kappa+i\phi_\kappa|^2\cos\delta)\ . \qquad (14)$$

For small ϵ_κ and ϕ_κ one can neglect the last two terms in Eq. (14) and the amplitude of the second harmonic is given by $4CE_0^2(|r_+^2|+|r_-^2|)J_2(A)$. Furthermore, n_+n_- in the denominators in Eq. (9) can be replaced by κ_1 [see also Eq. (6)] while the numerators become $-i\kappa_2/(\kappa_1)^{1/2}$. Thus both ϵ_κ and ϕ_κ are proportional to the magnetization.

III. EXPERIMENTAL RESULTS

A. Resistivity

Figure 3 is a plot of the resistivities of Ni-SiO_2 granular films as a function of composition at two temperatures. At high nickel concentration the resistivity increases relatively slowly with decreasing Ni concentration and has a small positive temperature coefficient. At 60 vol% Ni concentration and below the resistivity increases rapidly with decreasing concentration. In this range the temperature coefficient of the resistivity becomes negative and its absolute value increases with decreasing nickel concentration. The detailed dependence of the resistivity on the temperature T is shown in Fig. 4 for four nickel concentrations close to 50 vol%. The resistivities, plotted against $1000/T$, show a decreasing slope going towards low temperatures. Some of the samples seem to approach a constant slope from which an activation energy can be estimated.

B. Magnetoresistance

In Fig. 5, we show two curves of $\Delta\rho/\rho_0$ as a function of a (parallel) magnetic field for a 50 vol% Ni sample as measured with a bridge circuit and plotted on an X-Y recorder. The two curves were measured with a transverse field (perpendicular to the current flow) and differ considerably at low fields; the one measured at 125 °K approaching the origin with almost zero slope while the higher temperature one shows a relatively large slope. At high fields both curves show a relatively small field

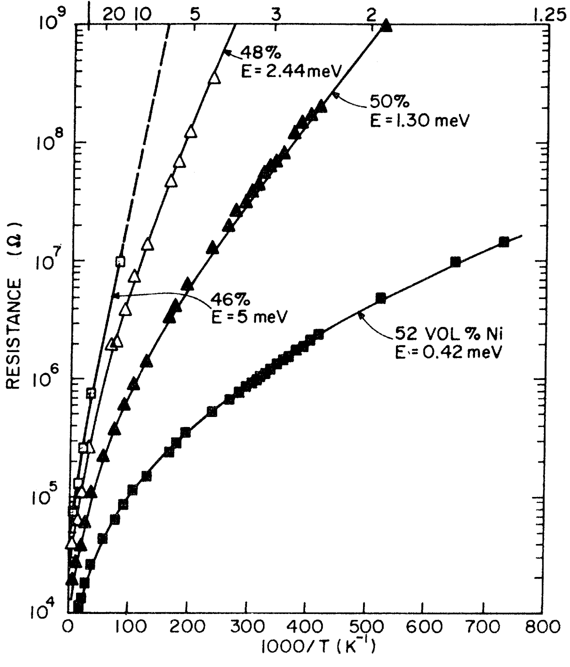

FIG. 4. Resistance vs $1000/T$ for 46, 48, 50, and 52 vol% Ni.

dependence. The longitudinal magnetoresistance curves (not shown here) show the same general behavior. Both the transverse and the longitudinal magnetoresistance were negative over the whole temperature range measured.

The values of the relative magnetoresistance for the transverse case are shown in Fig. 6 as a function of temperature for several Ni concentrations. These values were calculated from curves like those shown in Fig. 5 at a field of 4000 Oe. We notice several interesting features of these curves. The curves for the samples which contain 44 vol% nickel or less show a steady rise with decreasing temperature, while those for 54.5 vol% Ni or more are relatively flat at the higher temperatures and increase rapidly only below about 160 °K. The four curves for the intermediate nickel concentrations show a rise with decreasing temperature both at the high and low end of the temperature range shown but in addition they also exhibit an extended plateau at intermediate temperatures. The values of the magnetoresistance for these four samples at a field of 270 Oe are given in Fig. 7. Comparing this figure with Fig. 6, we see that the plateaulike behavior is now replaced with a sharp decrease in $\Delta\rho/\rho_0$, giving rise to pronounced maxima. At temperatures below that for which the maxima occurred a small hysteresis was observed in the field dependence of the magnetoresistance. The temperature at which these maxima occur is a very strong function of composition. Figure 8 shows the composition dependence of the small-field magnetoresistance at four temperatures. The common feature of these curves is the sharp peak in $\Delta\rho/\rho_0$ as a function of composition. The positions of these peaks are temperature dependent, moving towards lower nickel concentrations with decreasing temperature. In Fig. 9, the values of the small field longitudinal magnetoresistance are plotted vs the composition at 50 and 77 °K. For comparison the values of the transverse magnetoresistance at 77 °K are also given. As can be seen these two curves have more or less the same composition dependence even though the absolute value of the transverse magnetoresistance is somewhat higher. The most interesting feature of the data at 77 °K is the appearance of a shoulder at 50–52 vol% Ni concentration. As can be seen in the figure, at 50 °K this shoulder evolves into a peak and almost obstructs the temperature-dependent peak (at approximately 43 vol% Ni). The position of this new peak is essentially temperature independent while its magnitude increases with decreasing temperatures. Such peaks at 50–52 vol% Ni concentration were found at higher temperatures as well in the $\Delta\rho/\rho_0$ vs composition data taken at intermediate magnetic fields. Figure 10 shows the longitudinal magnetoresistance at 4000 Oe and at low temperatures for several compositions. At the high-temperature end the curves increase with decreasing temperature. At lower temperatures some of the curves show a decrease. Like all the other features of the magnetoresistance data, this decrease was found to be more pronounced at lower magnetic fields.

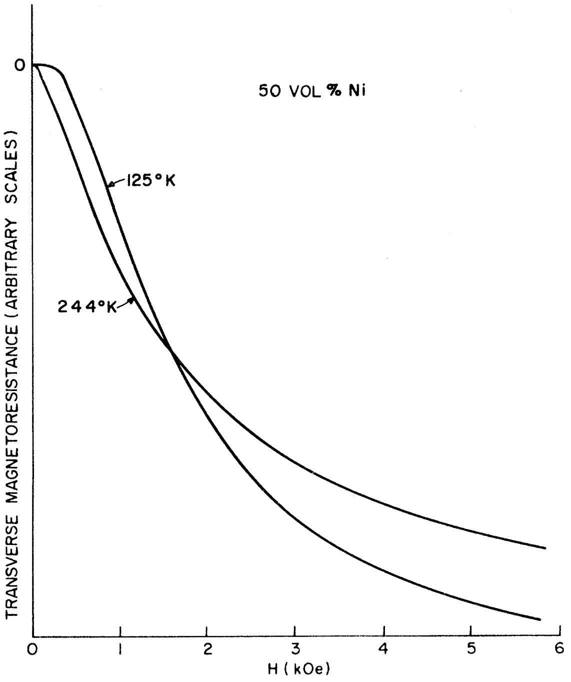

FIG. 5. Transverse magnetoresistance vs applied magnetic field for 50 vol% Ni.

C. Magneto-Optics

The magnetization of the Ni-SiO_2 samples as a function of a perpendicularly applied magnetic field was obtained by measuring the magneto-optic Kerr rotation, as explained in Sec. II B. At high nickel concentrations the magnetization increased linearly with the magnetic field up to close to its saturation value. Going towards lower nickel concentrations, the magnetization curves became more and more rounded. The linear portion became progressively smaller till it eventually disappeared. At room temperature this transition between linear and nonlinear behavior occurred between 50–58 vol% Ni. At higher temperatures the transition region shifted to somewhat higher Ni concentrations. In Fig. 11, the reciprocal of the initial slope of the relative magnetization at room temperature is plotted vs Ni concentration. At high Ni concentrations the data show a decrease with decreasing concentration, however, below 52 vol% Ni this trend is reversed and the data show an increase with a mini-

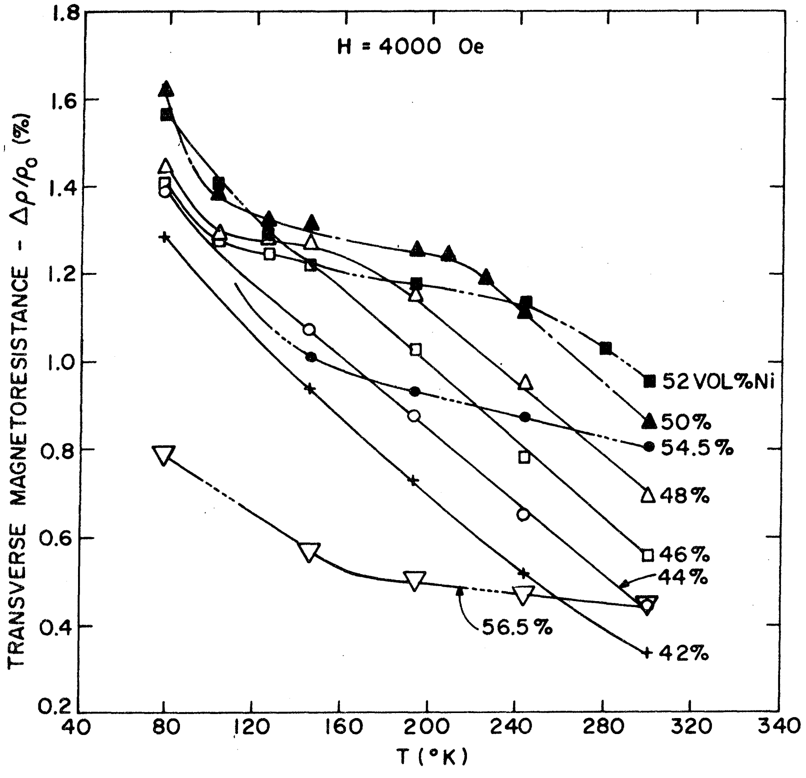

FIG. 6. Transverse magnetoresistance vs temperature at 4000 Oe.

mum at about 52 vol% Ni. This behavior was found at higher temperatures as well, with the position of the minimum shifting towards higher nickel concentrations. Figure 12 shows the saturation values of the measured Kerr rotation at room temperature. At high Ni concentrations the data

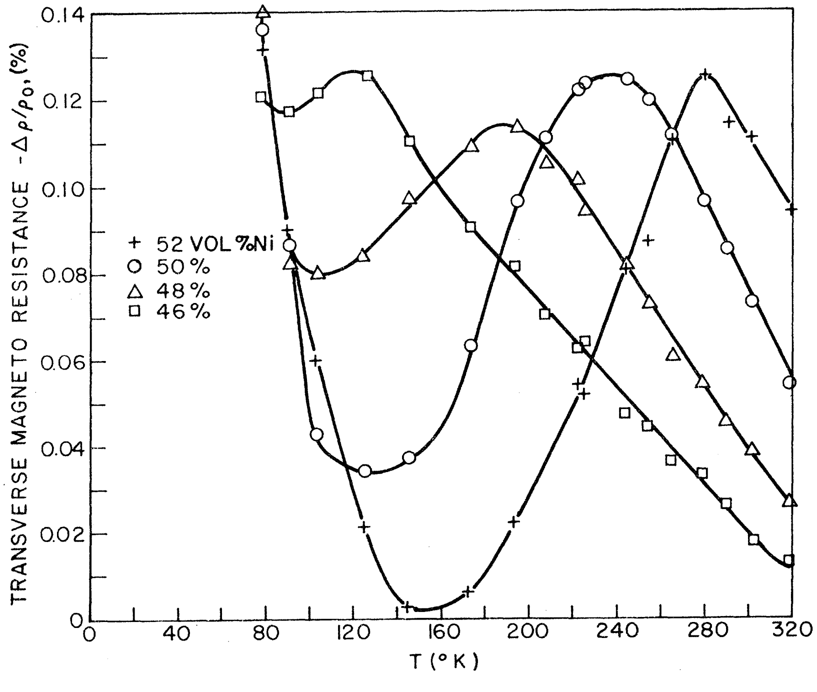

FIG. 7. Transverse magnetoresistance vs temperature at 270 Oe.

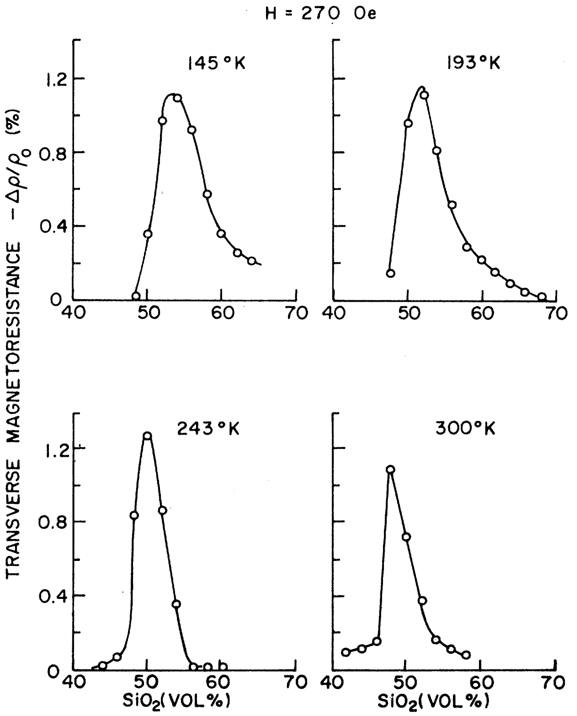

FIG. 8. Comparison of transverse magneotresistance vs composition (270 Oe) for four temperatures.

show an approximately linear decrease with decreasing Ni concentration. At lower concentrations the data decrease more gradually and depart from linearity.

IV. DISCUSSION

A. Resistivity

For specimens with compositions up to about 40 vol% SiO$_2$ the resistivity was very nearly independent of temperature. Furthermore assuming the ρl product to be about $2\times 10^{-11}\ \Omega\,\mathrm{cm}^2$ independent of composition, the effective electronic mean free path l varies from about 20 Å at 10 vol% SiO$_2$ to about 0.2 Å at 40 vol% SiO$_2$. Such behavior is very similar to that observed for granular superconductors[1] in which charge transport was attributed to tunneling between grains. The mean free path can then be related to the intergrain tunneling probability t by the following relation[1]:

$$l = td/(1-t)\,, \tag{15}$$

where d is the grain size. A rough estimate of the tunneling barrier height and Fermi energy can be obtained from simple tunneling theory[13] which yields for t,

$$1/t = 1 + [(E_F + U)^2/4E_F U]\sinh^2(\beta a)\,, \tag{16}$$

where E_F is the Fermi energy, U the height of the barrier above the Fermi surface, a is the width of the tunneling barrier, $\beta = (2mU/\hbar^2)^{1/2}$, m is the electronic mass, and $\hbar$ is Planck's constant divided by 2π. Assuming each grain to be a cube of width

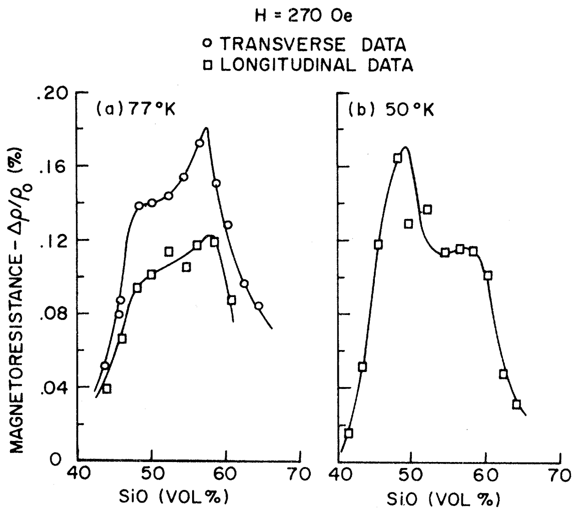

FIG. 9. Transverse and longitudinal magnetoresistance (270 Oe) vs composition at 77 and 50 °K.

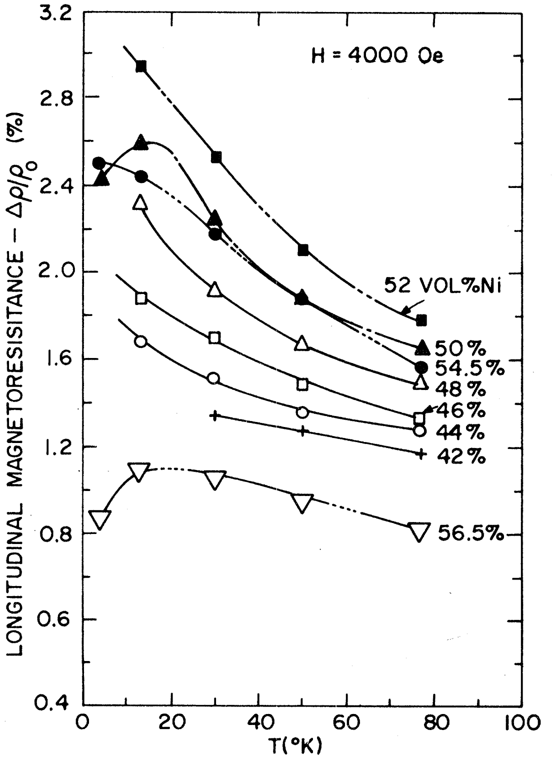

FIG. 10. Longitudinal magnetoresistance vs T ($H = 4000$ Oe).

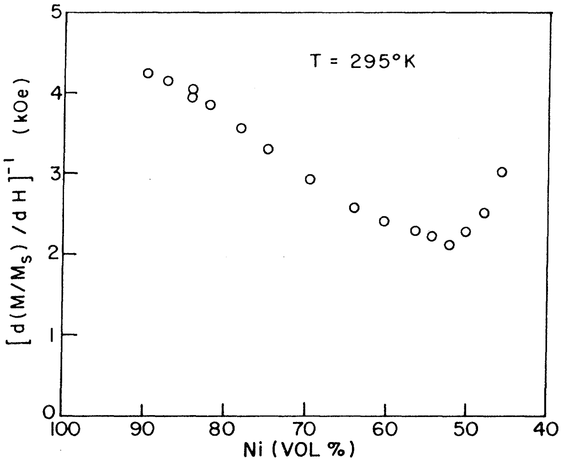

FIG. 11. Reciprocal slope of the normalized magnetization curve vs composition at 295 °K.

d encased in a sheath of SiO_2 of thickness $\frac{1}{2}a$, combining Eqs. (15) and (16) gives for the resistivity ρ_t due to the tunneling barrier

$$\rho_t = (\rho l/d)[(E_F + U)^2/4E_F U] \sinh^2(\tfrac{1}{3}\beta dx) , \qquad (17)$$

where x is the volume fraction of SiO_2. When $\frac{1}{3}\beta dx$ is greater than about 1.5

$$\rho_t = (\rho l/d)[(E_F + U)^2/4E_F U] \exp(\tfrac{2}{3}\beta dx) . \qquad (18)$$

The resistivity ρ is given by

$$\rho = \rho_{Ni} + \rho_t , \qquad (19)$$

where ρ_{Ni} is the resistivity of clean nickel ($\approx 7.8 \times 10^{-6}$ Ω cm). Figure 13 is a semilogarithmic plot of the tunneling resistivity $\rho - \rho_{Ni}$ against x. The straight line drawn through the data yields a barrier height U of about 0.5 eV for an assumed particle size of 50 Å. Assuming a value for ρl of 2×10^{-11} $\Omega\,cm^2$ yields a Fermi energy of about 4 eV. These values are reasonable considering the simplicity of the model. The sharp rise of ρ above the straight line for values of $x \gtrsim 0.3$ can probably be attributed to an increase in the effective barrier height as the thickness of the SiO_2 barrier increases.

For SiO_2 content above 40 vol%, the resistivity becomes increasingly temperature dependent. At low temperatures the data can be interpreted in terms of a small activation energy (see Fig. 4). Hill[14] has developed a model for temperature-dependent tunneling. The temperature variation of the resistance he derives is qualitatively similar to our measured dependence. However, the $\sin(\pi\beta kT)$ variation given in Eq. (5) of Ref. 14 is inconsistent with our data.

B. Magnetoresistance

Inspecting our data on magnetoresistance we notice first of all that the longitudinal magnetoresistance is negative. This is contrary to the known experimental fact[15] that the longitudinal magnetoresistance of nickel is positive over the whole temperature range covered by our measurements and becomes negative only in a narrow region around T_C. The transverse magnetoresistance of nickel, on the other hand, is negative and its relative magnitude at high magnetic fields is of the order of a few percent. This is seemingly in qualitative agreement with our present data on the transverse magnetoresistance at high fields and one may be tempted to interpret the transverse data as due to the magnetoresistance of the nickel grains. However, the resistivity measurements show that the resistivity ρ is dominated by the tunneling resistivity ρ_t which is orders of magnitude higher than the resistivity of nickel ρ_{Ni}. Thus, even though the relative magnetoresistance is only a few percent, the corresponding change in ρ is much higher than the total resistivity of nickel. Accordingly we conclude that the electronic tunneling probability t and ρ_t are magnetic-field dependent. Such a field dependence of the tunneling probability can arise from the fact that as an electron tunnels into a neighboring grain its spin must be rotated whenever the moments of the grains are not aligned. This also explains qualitatively the occurrences of the maxima in the plot of the small-field magnetoresistance vs temperature in Fig. 7. Because of the weak coupling between the grains, at high temperatures the moments of the grains are disordered. A weak magnetic field is insufficient to align them

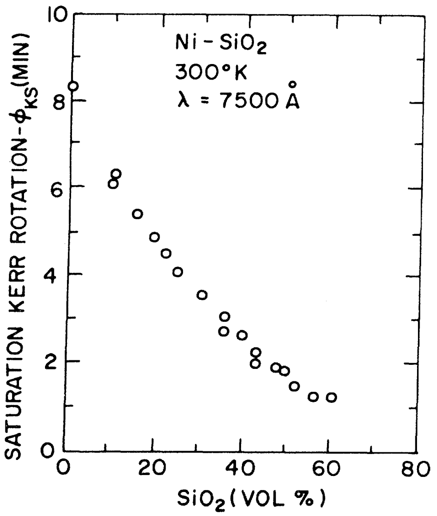

FIG. 12. Saturation Kerr rotation vs composition.

appreciably and thus the magnetoresistance is small. At progressively lower temperatures the alignment due to the field becomes more effective, with a corresponding increase in magnetoresistance. At a certain temperature, which we identify with an ordering temperature T_M, there is a spontaneous alignment between the grains. This is also evidenced by the appearance of a small hysteresis in the $\Delta\rho/\rho_0$-vs-H curves. As the temperature decreases even lower, the alignment becomes more effective and is affected but little by the external field. This is analogous to the occurrence of a peak in the magnetoresistance of ferromagnets at the Curie point due to spin disorder scattering.[15] The difference here is, however, that T_M is associated with the transition from a ferromagnetic state of the ensemble to a superparamagnetic state. In the superparamagnetic state the individual nickel grains retain their magnetic moments, but because of the weak interaction between the grains the ensemble as as a whole becomes disordered.

In order to obtain a simple description of the magnetoresistance and to provide a means for quantitatively comparing the magnetoresistance data and magnetization, we adopt a heuristic approach. We assume (i) a uniform grain size and (ii) that the field-dependent part of the tunneling probability is proportional to the degree of correlation of the moments of neighboring grains averaged over all configurations, $\langle \vec{\mu}_1(H) \cdot \vec{\mu}_2(H) \rangle / \mu^2$, where $\vec{\mu}_i$ is the magnetic moment of the ith grain and $|\mu_i| = \mu$. Ignoring scattering within the grains the conductivity σ can then be written

$$\sigma(T, H) = \sigma_0(T) + \sigma_1(T) \langle \vec{\mu}_1 \cdot \vec{\mu}_2 \rangle / \mu^2 , \qquad (20)$$

where σ_0 is the conductivity in the absence of the magnetic field and σ_1 is a proportionality factor. The magnetic field enters into Eq. (20) only through the change $\Delta \langle \vec{\mu}_1 \cdot \vec{\mu}_2 \rangle$ of this average due to the magnetic field. The magnetoresistance can now be written

$$\Delta\rho/\rho_0 \approx -\sigma_1(T) \Delta \langle \vec{\mu}_1 \cdot \vec{\mu}_2 \rangle / \mu^2 \sigma_0(T) . \qquad (21)$$

As a first approximation a molecular field theory can be used to express $\langle \vec{\mu}_1 \cdot \vec{\mu}_2 \rangle$. The magnetic moments of the grains are very large compared to

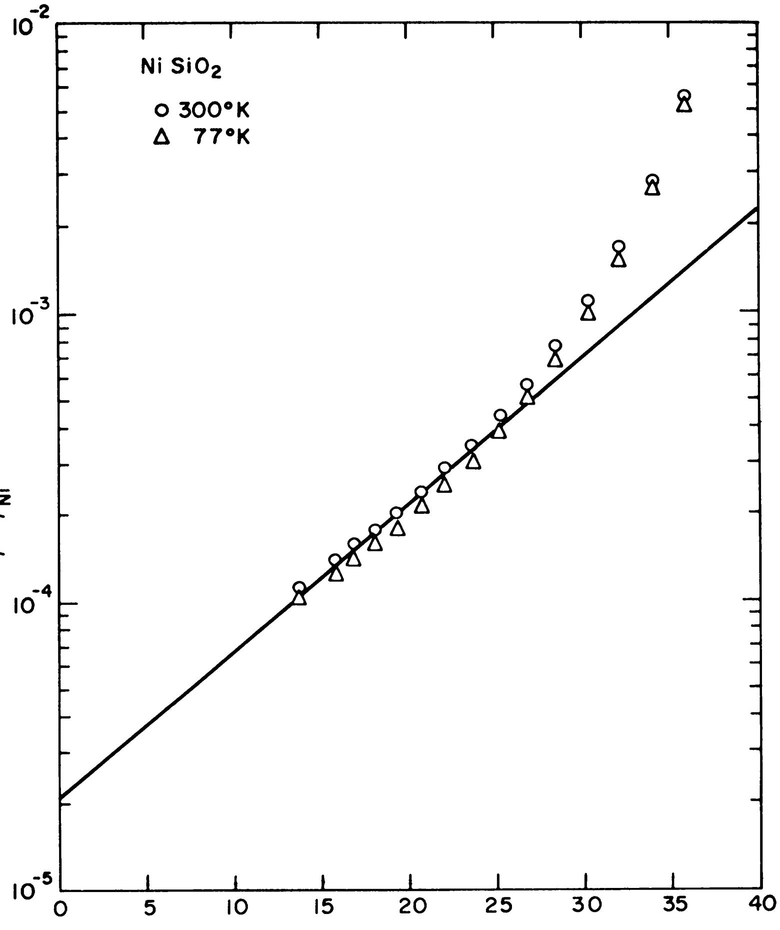

FIG. 13. $\rho - \rho_{\rm Ni}$ vs composition.

the moment of a single atom and thus a classical theory should be adequate to describe the system. Carrying out the indicated average, we find that $\langle \vec{\mu}_1 \cdot \vec{\mu}_2 \rangle$ is $\mu^2[L(\alpha)]^2$, where $L(\alpha)$ is the Langevin function and is given by

$$L(\alpha) = \coth\alpha - 1/\alpha \;, \tag{22}$$

with

$$\alpha = \mu(H + \lambda M)/kT = (\mu H/kT) + 3(T_M/T)(M/M_s) \;. \tag{23}$$

Here H is the applied (parallel) magnetic field, M is the magnetization, λ is the molecular field constant, and k is Boltzmann's constant. The saturation magnetization $M_s = N\mu$, where N is the number of grains/unit volume.

Figure 14 shows a curve calculated from equations (21)–(23) together with the experimental results (triangles) for the 48-vol%-Ni sample. The fit was obtained by choosing $T_M = 188$ °K, $\mu = 1 \times 10^{-16}$ erg Oe^{-1}, and $\sigma_1 = 8 \times 10^{-4}$ $(\Omega\,\mathrm{cm})^{-1}$. As can be seen the experimental results are reasonably reproduced by the calculated curve except at T_M and at low temperatures. At T_M the calculated curve has a sharp peak whereas the observed maximum is broad. This is believed to result from a small variation in the magnetic moment of the grains and the spatial variation of T_M due to nonuniform particle sizes and tunneling barriers. The sharp increase of the measured magnetoresistance at low temperatures may result from the temperature dependence of σ_1 and cannot be evaulated within the framework of the present model. Similar fits could be obtained for the rest of the data shown in Fig. 7, with μ increasing slowly with increasing nickel concentration. Assuming spherical grains, the grain size estimated from the magnetic moment varies between 50–60 Å in agreement with the estimates from the electron micrographs.

The composition dependence of the magnetoresistance, Figs. 8 and 9, are all consistent with the above interpretation. In all cases we observe a maximum in $\Delta\rho/\rho_0$ for that sample which is closest to its ordering temperature.

The low-temperature behavior of the magnetoresistance is not well understood. As can be seen in Fig. 6, all the samples exhibit a rise in the magnetoresistance at low temperatures. For the samples whose ordering temperature is below 70 °K (42–46 vol% Ni), $\Delta\rho/\rho_0$ rises with almost constant slope exhibiting only a small change in the slope at low temperatures. For the samples whose ordering temperature is within or above the temperature range of the figure, $\Delta\rho/\rho_0$ shows a flat region and again a rise at low temperatures. It almost looks as though the flat region is the result of the two opposing trends—the decrease of $\Delta\rho/\rho_0$ below T_M and the increase at low temperatures. The behavior of the longitudinal magnetoresistance (Fig. 10) is even more complicated. It is possible that the low-temperature behavior of the magnetoresistance is closely connected with the temperature-dependent tunneling process.

C. Magnetization

The relative magnetization as a function of a perpendicular magnetic field H was measured by the magneto-optical Kerr rotation. The measurements were performed at room temperature and slightly above (290–360 °K). At these temperatures the crystalline anisotropy of nickel[16]

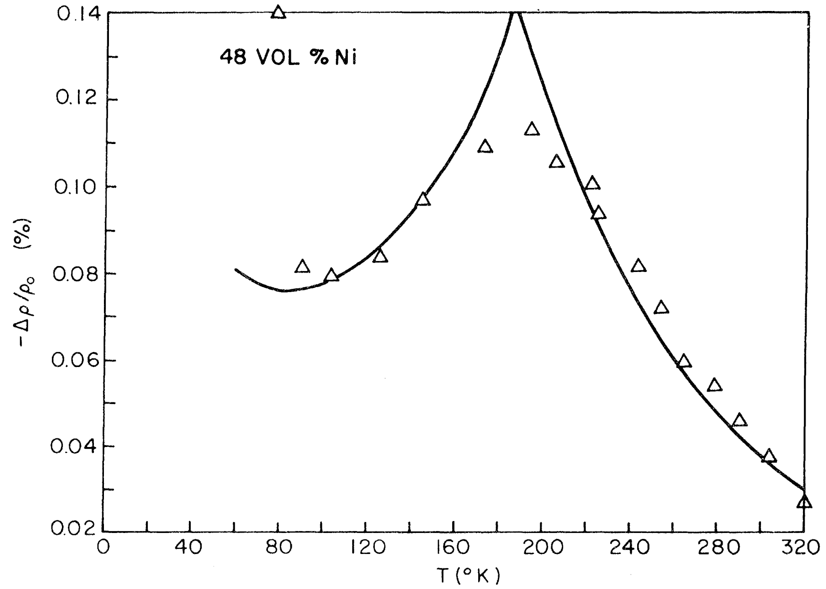

FIG. 14. Comparison of $\Delta\rho/\rho_0$ vs T with theory (48 vol% Ni).

is negligible and thus the magnetization of a thin ferromagnetic nickel film is expected to rise linearly as $H/4\pi$ and to curve slightly only close to its saturation value. Such a behavior was indeed observed for samples with high nickel concentration. In this range the slopes of the measured ϕ_K-vs-H (and thus the M-vs-H) curves were constant up to close to the saturation values. Going towards lower Ni concentrations the magnetization curves started to deviate from the ferromagnetic behavior and become more and more rounded. At 295 °K, the curve for 48 vol% Ni has already no straight portion at all and closely resembles a magnetization curve for a superparamagnetic[17] specimen. The curve for this specimen was indeed very well reproduced using a molecular field theory and equating M/M_s to $L(\alpha)$ given by Eqs. (22) and (23), where H in Eq. (23) now included the demagnetizing field $-4\pi M$. These calculated values are shown by points in Fig. 15 together with the measured magnetization curve. The parameters μ and T_M used for the fit were the same as those used to fit the magnetoresistance data of the 48-vol%-Ni specimen (Fig. 14). Similar fits were obtained at somewhat lower Ni concentrations. At higher temperatures the transition region moved to slightly higher concentrations.

For a film in a magnetic field perpendicular to its surface (demagnetizing coefficient $= 4\pi$), the normalized initial slope of the magnetization curve is sensitive to the magnetic state of the specimen. Thus if

$$S_n = \left(\frac{1}{M_s} \frac{dM}{dH_0} \right)^{-1}_{H_0=0} ,$$

we have in the ordered state $M = H_0/4\pi$ for $H_0 < 4\pi M_s$ (H_0 = the applied field) and $S_n = 4\pi M_s \chi$ (a decreasing function of SiO_2 concentration). If $T > T_M$ and the specimen exhibits superparamagnetic behavior, then $M = \chi/(1+4\pi\chi)\, H_0$ and $S_n = 4\pi M_s\,(1+1/4\pi\chi)$,

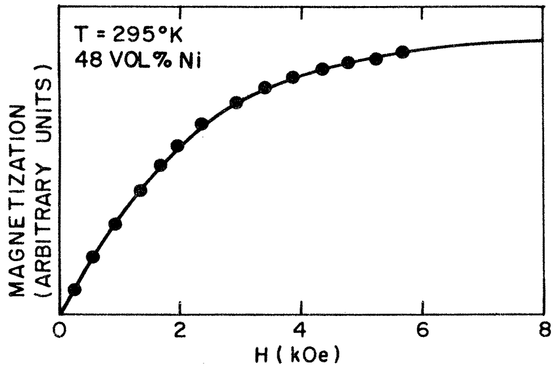

FIG. 15. Comparison of magnetization data (solid line) vs theory (circle), 48 vol% Ni, $T = 295$ °K.

where χ is the initial susceptibility. Thus in the superparamagnetic state S_n is larger by the factor $(1+1/4\pi\chi)$ than its value in the ordered state. Therefore if, at a given temperature T, S_n is plotted as a function of Ni concentration there will be a break in the curve at that concentration for which $T = T_M$. The ordering temperature T_M as a function of concentration, can then be determined. Figure 11 is a plot of the reciprocal slope measured at $T = 295$ °K. At 52 vol% Ni a clear break (a minimum in fact) is observed in the data. We therefore take $T_M = 295$ °K for 52 vol% Ni. At high temperatures, the minimum occurred at higher nickel concentrations.

V. CONCLUSIONS

The foregoing results indicate that, depending on temperature and composition, the Ni-SiO_2 system can exist in an ordered phase in which the specimen as a whole is ferromagnetic and a disordered phase in which the specimen is superparamagnetic. Figure 16 is a phase diagram for the granular Ni-SiO_2 system. The solid line shows the ferromagnetic to superparamagnetic transition temperature as a function of composition. The circles were obtained from the magnetoresistance data and the triangles from the inverse slope of the magnetization curves. It can be seen that the two criteria lead to mutually consistent results. The Curie temperature of 100% Ni is also shown (square). The dashed horizontal line at 630 °K represents the upper limit for the transition to the phase in which each grain is paramagnetic. The actual phase boundary which is determined by the Curie temperature of the individual grains is expected to drop below 630 °K as the nickel concentration decreases because of size effects.[9,10]

The behavior of granular nickel is, in some respects, similar to that of the Ni-Cu alloys.[18,19] In the granular system the giant moment arises from grains of fcc Ni containing of the order of 10^4 atoms rather than from clusters containing of the order of ten Ni atoms in the case of Ni-Cu. Thus, even at temperatures well above the measured ordering temperatures, the condition $\mu H/kT \gtrsim 1$ can be achieved for granular Ni at relatively small magnetic fields, so that the characteristic Langevin dependence of the magnetization can be readily observed.

According to the theory of Fibich and Ron[19] the ferromagnetic coupling between Ni clusters is dominated by interactions involving the conduction electrons of the Ni-Cu lattice. For granular Ni the experimental results suggest that the dominant interactions involve electrons which tunnel between adjacent grains. If this is so, it can be expected that the interaction strength is a function of the intergrain tunneling probability and T_M is a sensi-

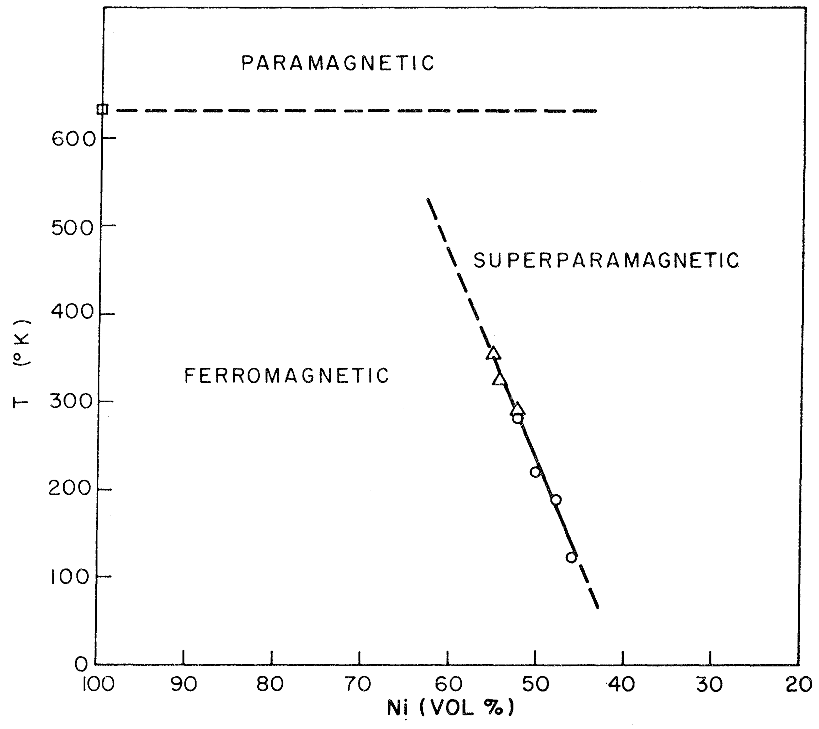

FIG. 16. Magnetic phase diagram for $Ni_x(SiO_2)_{1-x}$.

tive function of the composition. In fact the decrease of T_M with decreasing Ni concentration is about three times larger for granular Ni than for the Ni-Cu alloys.

It is interesting to note that at a concentration of about 50 vol% Ni the value of the molecular field constant λ obtained from the values of T_M, μ, and M_s was 4.15, very close to $\frac{4}{3}\pi$. Thus, the molecular field is of the same order of magnitude as the Lorentz field. Although this may suggest that at these concentrations the observed ordering is due to magnetic dipole interactions, the insufficiency of available evidence and the theoretical difficulties[20,21] encountered lead us to believe such a conclusion to be premature.

Finally, the authors feel that the temperature T_M is an ordering temperature and not a blocking temperature.[21] The blocking temperature T_B can be estimated using the relation[21]

$$\tfrac{1}{2}CV \approx 25kT_B ,$$

where CV is the height of the barrier opposing thermal fluctuations, V is the volume of a grain, and C is the dominant anisotropy energy. For nickel the largest value of C possible is $2\pi M_s^2$ which would result from shape anisotropy and a demagnetizing coefficient of 4π. Thus T_B for a 60-Å particle size is about 30 °K, far less than any observed value of T_M.

ACKNOWLEDGMENTS

The authors would like to thank G. D. Cody for suggesting the existence of granular ferromagnetic systems by analogy with granular superconductivity. They would also like to thank R. W. Cohen and B. Abeles for many helpful discussions, M. D. Coutts for electron microscope measurements, and J. P. Pellicane for the preparation of the specimens.

---

*On leave of absence from the Hebrew University, Jerusalem, Israel.

[1] B. Abeles, R. W. Cohen, and G. W. Cullen, Phys. Rev. Letters 17, 632 (1966); R. W. Cohen, B. Abeles, and G. S. Weisbarth, *ibid.* 18, 336 (1967); B. Abeles, R. W. Cohen, and W. R. Stowell, *ibid.* 18, 902 (1967).

[2] N. C. Miller and G. A. Shirn, Appl. Phys. Letters 10, 86 (1967).

[3] J. F. Henrickson, G. Krauss, R. N. Tauber, and D. J. Sharp, J. Appl. Phys. 40, 5006 (1969).

[4] W. E. Masker, S. Marcelja, and R. D. Parks, Phys. Rev. 188, 745 (1969).

[5] R. W. Cohen and B. Abeles, Phys. Rev. 168, 444 (1968).

[6] R. W. Cohen and J. I. Gittleman, Phys. Rev. 176, 500 (1968).

[7] J. J. Hanak and J. I. Gittleman, Physica 55, 555 (1971); J. J. Hanak, J. Mater. Sci. 5, 964 (1970).

[8] D. Schultze, Naturwiss. 47, 128 (1960).

[9] C. R. Abeledo and P. W. Selwood, J. Appl. Phys. 32, 229S (1961).

[10] Y. Goldstein and J. I. Gittleman, Solid State Commun.

9, 1197 (1971).

[11] S. N. Jasperson and S. E. Schnatterly, Rev. Sci. Instr. 40, 761 (1969).

[12] See, for instance, M. J. Freiser, IEEE Trans. Magnetics 4, 152 (1968).

[13] See, for instance, V. Rojansky, *Introductory Quantum Mechanics* (Prentice-Hall, Englewood Cliffs, N.J., 1938), Chap. 6.

[14] R. M. Hill, Proc. Roy. Soc. (London) A309, 377 (1969).

[15] See, for instance, R. M. Bozorth, *Ferromagnetism* (Van Nostrand, Princeton, N.J., 1951), Chap. 16.

[16] R. M. Bozorth, *Ferromagnetism* (Van Nostrand, Princeton, N.J., 1951), Chap. 12.

[17] A. H. Morrish, *The Physical Principles of Magnetism* (Wiley, New York, 1965), Chap. 7, Sec. 3.

[18] J. S. Kouvel and J. B. Comly, Phys. Rev. Letters 24, 598 (1970).

[19] M. Fibich and A. Ron, Phys. Rev. Letters 25, 296 (1970).

[20] L. Onsager, J. Am. Chem. Soc. 58, 1486 (1936).

[21] A. H. Morrish, *The Physical Principles of Magnetism* (Wiley, New York, 1965), Chap. 7, Sec. 3, p. 362.

PHYSICAL REVIEW B VOLUME 5, NUMBER 9 1 MAY 1972

The $AuAl_2$-$AuGa_2$-$AuIn_2$ Problem: Knight Shifts and Relaxation Times in Their Pseudobinary Alloys

G. C. Carter, I. D. Weisman, L. H. Bennett
Institute for Materials Research,
National Bureau of Standards, Gaithersburg, Maryland 20760
and
R. E. Watson*
Brookhaven National Laboratory,† *Upton, New York* 11973

(Received 25 June 1971)

The nuclear-magnetic-resonance (NMR) and susceptibility behavior of the intermetallic compound $AuGa_2$ differs anomalously from the isoelectric and isostructural compounds $AuIn_2$ and $AuAl_2$. In an effort to test and extend the explanation offered by Jaccarino *et al.* and by Switendick and Narath, spin-lattice relaxation times and Knight shifts have been measured as a function of temperature and composition for the $AuAl_2$-$AuGa_2$, $AuAl_2$-$AuIn_2$, and $AuGa_2$-$AuIn_2$ pseudobinary alloy systems. At high temperature, the solute X (Al, In, Ga) resonance properties are dominated by the host. Satellite resonances are observed with temperature dependences differing from the main resonance. The results are partially explainable on the basis of an average-band model and partially on a local atom model. The role of the Au d bands is discussed. Metallurgical results on alloying are obtained using the NMR data.

I. INTRODUCTION

The three intermetallic compounds, $AuAl_2$, $AuGa_2$, and $AuIn_2$, are at once interesting and confusing. The three, all crystallizing in the fluorite structure, display similarities and dissimilarities which, to date, would seem to be incompatible. The most striking difference[1] among the three is the fact that $AuGa_2$ has a strongly temperature-dependent susceptibility χ and Knight shift $\mathcal{K}$, the latter reversing sign, whereas the other two compounds display temperature independence. Explanation of the $AuGa_2$ data apparently requires a model,[1] henceforth denoted JWWM (after Jaccarino, Wernick, Weger, Menth), involving a very substantial modification with temperature of the band character at the Fermi surface.

Switendick and Narath[2] calculated the electronic band structures of the three compounds. They uncovered a feature of the $AuGa_2$ bands not present in the others, which could lead to a band-repopulation effect, which in turn could explain the Knight-shift behavior but not necessarily the susceptibility. Such an effect, or in fact, any band modification yielding the Knight-shift variation, would be expected to be reflected in the electrical properties of this metal. The thermoelectric power is anomalous.[3] But Hall-effect,[3] resistivity,[3,4] and magnetoresistivity[4] measurements display no anomalous variation with temperature in this compound. These facts are central to the "puzzle" of the AuX_2 compounds.

In an effort to further explore this matter, we have obtained Knight-shift and relaxation-time results at host and impurity-X sites in the dilute pseudobinary alloys formed by the AuX_2 compounds with each other. The results are consistent with the JWWM model. They supply no obvious justification or refutation of the existing band calculation for the $AuGa_2$ behavior, but they add some in-

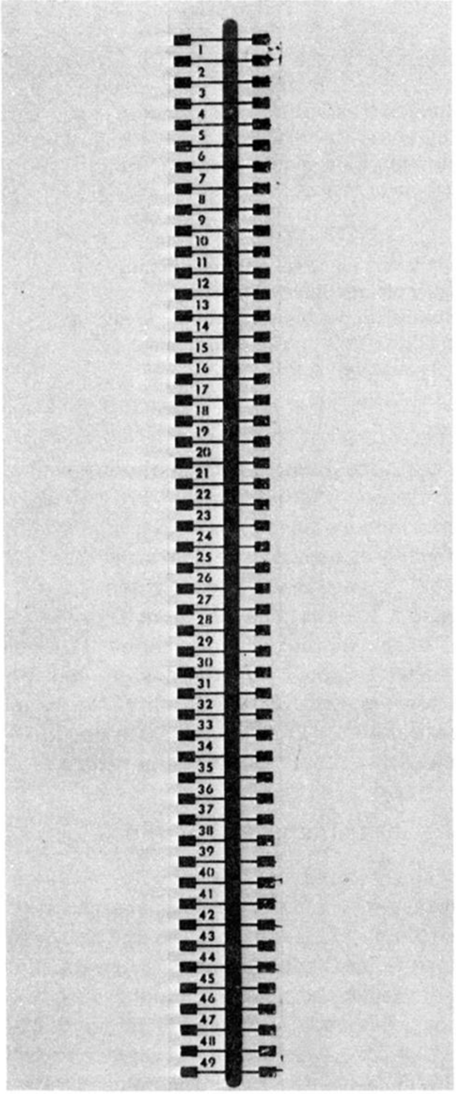

FIG. 1. Sputtered Ni-SiO_2 specimen. Sample No. 1, SiO_2 rich; sample No. 49, Ni rich.